Efficient Nonlinear Frequency Conversion in an All-Resonant Double-Λ System

Andrew J. Merriam, S. J. Sharpe, M. Shverdin, D. Manuszak, G. Y. Yin, and S. E. Harris
Edward L. Ginzton Laboratory, Stanford University, Stanford, California 94305
(Received 3 February 2000)

We demonstrate efficient, pulsed, gas-phase, nonlinear frequency conversion in a quadruply resonant, double-Λ system and, simultaneously, verify theoretical predictions of Rabi-frequency matching unique to absorbing nonlinear media. This system is used to up-convert ultraviolet light at 233 nm to the vacuum ultraviolet at 186 nm in atomic Pb vapor with small-signal conversion efficiencies exceeding 30% and with modest atomic density-length (NL) products (scale 10^{14} cm^{-2}) and optical power densities ($10-100$ kW/cm^2).

PACS numbers: 42.50.Gy, 42.50.Hz, 42.65.Ky, 42.79.Nv

It has been shown that the techniques of electromagnetically induced transparency (EIT) may greatly improve the efficiency of gas-phase nonlinear optical processes [1,2]. EIT facilitates the preparation of near-maximal coherence of a dipole-forbidden transition without absorption or self-phase modulation of the applied fields; the phase-coherent atomic ensemble thus created acts as a strong local oscillator which may mix with the spectral components of the applied fields to generate a corresponding spectrum of sum or difference frequencies. Previous work in both the gas [1,2] and solid [3] phases has focused on the reactive case (i.e., large detuning of the generated frequency from any resonances and near-lossless propagation) and has demonstrated efficient parametric frequency conversion to the ultraviolet and vacuum ultraviolet (VUV).

In this Letter, we explore gas-phase, nonlinear frequency up-conversion in a quadruply resonant atomic system. This atom-field combination is known as a resonant double-Λ configuration and has been studied in the context of EIT [4], lasers without inversion [5], and nonlinear optics [6]. The short-wavelength up-converted radiation is generated directly on resonance under conditions where, in the absence of the other fields, it would be strongly absorbed. We demonstrate, however, that through the up-conversion process, the atomic system renders itself transparent to all four fields. Transparency is achieved once the complex ratio of Rabi frequencies in each Λ-channel is equal and, once transparent, no further changes to the relative phase or amplitude of each field occur [7]. Additionally, we observe important saturation mechanisms which may limit the generated radiation intensity attainable with this type of frequency converter.

We begin with a brief theoretical discussion of this work. We consider a four-state system in the rotating wave approximation, as shown in the inset in Fig. 1. The coupling laser, tuned to the $|2\rangle \rightarrow |3\rangle$ transition with Rabi frequency Ω_c (406 nm), and the probe laser, tuned to the $|1\rangle \rightarrow |3\rangle$ transition with Rabi frequency Ω_p (283 nm), adiabatically establish a large atomic coherence of the Raman transition, which is described by the off-diagonal density matrix element ρ_{12} [2]. A third laser field with radian frequency ω_e is tuned to resonance with the $|2\rangle \rightarrow |4\rangle$ transition and mixes with the coherence to generate a fourth field at ω_h resonant with the $|1\rangle \rightarrow |4\rangle$ transition. The (small-signal) electric-field attenuation coefficients of the mixing and generated fields are $\alpha_e = N\sigma_e\rho_{22}/2$ and $\alpha_h = N\sigma_h\rho_{11}/2$, where N is the atom density, ρ_{jj} is the total fraction of atoms in state $|j\rangle$, and σ_e and σ_h are the single-atom, Doppler-broadened, resonant, absorption cross sections. The coherently trapped population is distributed according to $\rho_{11} = \Omega_c^2/(\Omega_c^2 + \Omega_p^2)$, $\rho_{22} = \Omega_p^2/(\Omega_c^2 + \Omega_p^2)$, and $\rho_{12} = -\Omega_p\Omega_c^*/(\Omega_p^2 + \Omega_c^2)$. With these definitions, in a plane-wave approximation and ignoring saturation effects and light shifts, the propagation equations for a quadruply resonant frequency converter from Ω_e (233 nm) to Ω_h (186 nm) are [2]

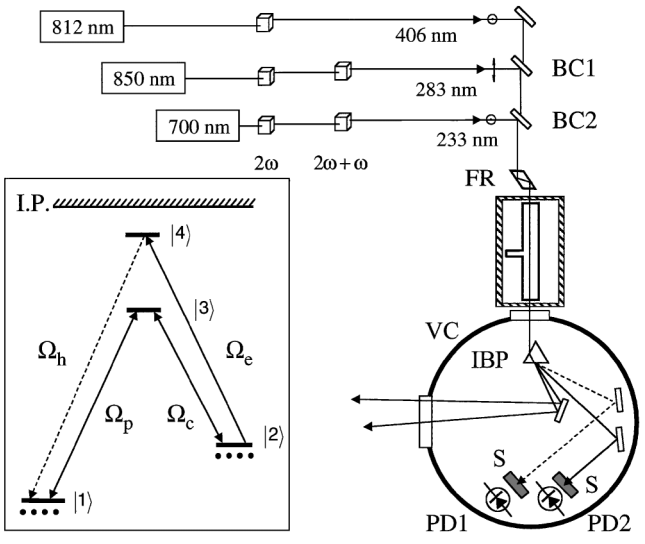

FIG. 1. Schematic diagram of the experimental apparatus. BC1, etc., described in main text. Inset: Energy-level diagram of the double-Λ system in ^{208}Pb vapor. Laser fields with Rabi frequencies Ω_p, Ω_c, and Ω_e are applied, and Ω_h is generated. State designations and energies: $|1\rangle$, $6p^2\ ^3P_0$, 0.0 cm^{-1} (ground); $|2\rangle$, $6p^2\ ^3P_2$, 10 650.3271 cm^{-1}; $|3\rangle$, $6p7s\ ^3P_1$, 35 287.2244 cm^{-1}; $|4\rangle$, $6p9s\ ^3P_1$, 53 511.1485 cm^{-1}. The ionization potential of Pb I is 59 819 cm^{-1} (7.42 eV).

 0031-9007/00/84(23)/5308(4)$15.00

$$\frac{\partial \Omega_e}{\partial z} + \alpha_e \Omega_e = -\frac{N\sigma_e}{2}\rho_{12}^{*}\Omega_h \exp(+i\Delta k z), \quad (1a)$$

$$\frac{\partial \Omega_h}{\partial z} + \alpha_h \Omega_h = -\frac{N\sigma_h}{2}\rho_{12}\Omega_e \exp(-i\Delta k z). \quad (1b)$$

Since k-vector matching of the interacting laser fields is automatically satisfied by resonant copropagating fields in the rotating wave approximation, $\Delta k = 0$. The solutions of Eqs. (1) with boundary conditions $\Omega_h(z = 0) = 0$ and $\Omega_e(z = 0) = \Omega_e(0)$ are

$$\frac{\Omega_h(z)}{\Omega_e(0)} = iN\sigma_h\rho_{12}\exp\left[-\frac{\alpha_T z}{2}\right]\frac{\sin(i\alpha_T z/2)}{\alpha_T} = \left(\frac{\Omega_p}{\Omega_c}\right)\left(\frac{\alpha_h}{\alpha_T}\right)(1 - e^{-\alpha_T z}), \quad (2a)$$

$$\frac{\Omega_e(z)}{\Omega_e(0)} = \frac{\alpha_h}{\alpha_T} + \frac{\alpha_e}{\alpha_T}e^{-\alpha_T z}, \quad (2b)$$

where $\alpha_T = \alpha_e + \alpha_h$. This solution assumes that the atomic coherence ρ_{12} established by the fields in the first Λ-channel is unaffected by the generation process; this is ensured by maintaining $\Omega_e(0)$ an order of magnitude less than Ω_p and Ω_c during the experiment.

The central result of this work is that, in the limit of many absorption lengths ($\alpha_T z \to \infty$), the nonlinear generation process matches the ratio of Rabi frequencies in each Λ-channel so that $\Omega_h(z)/\Omega_e(z) \to \Omega_p/\Omega_c$. The frequency conversion behavior predicted by Eq. (2) is dramatically different from that witnessed in earlier, far-detuned experiments [1]; no longer is there parametric power oscillation between fields as a function of distance into the nonlinear medium, but, rather, monotonic growth towards an asymptotic value. This result may be viewed as a special case of matched pulses [7] in a double-Λ system; atoms evolved into the coherent population-trapped eigenstate are invisible to any pair of optical frequency fields on the $|1\rangle \leftrightarrow |4\rangle$ and $|2\rangle \leftrightarrow |4\rangle$ transitions whose complex ratio of Rabi frequencies is Ω_p/Ω_c. Pairs of input fields which differ from this ratio undergo selective absorption of unmatched Fourier components and nonlinear generation until they conform to this ratio and are thereby decoupled from the medium. This behavior is quite different from the density invariance of previous resonant frequency conversion experiments caused by competition between four-wave mixing and two-photon absorption [8].

We now turn to a description of the experiment. A schematic diagram of the experimental setup is shown in Fig. 1. Three linearly polarized, coherent beams at 406, 283, and 233 nm are spatially and temporally overlapped by beam combiners BC1 and BC2, converted to circular polarization by a Fresnel rhomb FR, and propagate collinearly through the Pb atomic vapor contained in a heated sidearm cell. The output beams propagate $\sim$1 cm in atmosphere into a vacuum chamber VC (maintained $<$500 mTorr) and are dispersed by an isosceles Brewster prism IBP. The generated field at 186 nm and residual mixing field at 233 nm are directed onto sodium salicylate scintillators S. The fluorescence signals are sampled by fast photodiodes PD1 and PD2. Each waveform is digitized and downloaded to a computer. The data are analyzed, sorted by the pulse timing, and plotted; data with pulse timing overlap errors less than 5 ns are retained. The data shown in Figs. 2–5 are from individual events and are not averaged.

The laser setup is similar to that used in previous experiments [2,9]. All beams are collimated with intensity FWHM beam diameters of 2.0 mm (coupling laser, 406 nm, 30-ns pulse width), 2.12 mm (probe laser, 283 nm, 15-ns pulse width), and 1.24 mm (mixing laser, 233 nm, 15-ns pulse width). The area of the generated beam is inferred to be the same as that of the mixing laser. Laser frequencies are determined using a Burleigh Model 4500 pulsed wave meter with a maximum resolution of 0.01 cm^{-1} (300 MHz). Typical energies and (peak) Rabi frequencies for the probe, coupling, mixing, and generated lasers are 50 μJ (0.25 cm^{-1}), 50 μJ (0.30 cm^{-1}), 1 μJ (0.0148 cm^{-1}), and 0.1 μJ (5.31×10^{-3} cm^{-1}), respectively. (These beam energies are a factor of 200 lower than those employed in previous EIT-enhanced nonlinear optics experiments [1,2].)

The 186-nm vacuum ultraviolet radiation is generated as a collimated beam which propagates collinearly (i.e., on axis) with the three applied fields. Typical pulse energies are less than 1 μJ and are determined using a scintillator/photodiode combination which has been calibrated with known 233-nm beam energies [10].

The atomic vapor is 99.86% isotopically enriched ^{208}Pb metal (Oak Ridge National Laboratory), heated within a 25-cm-long fused quartz sidearm cell manufactured by Opthos Instruments. As in previous work [11], densities

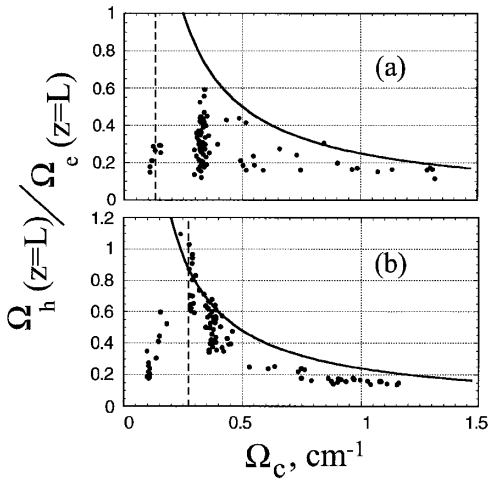

FIG. 2. Ratio of generated 186-nm and output 233-nm Rabi frequencies, at the exit of the cell $\Omega_h(z = L)/\Omega_e(z = L)$, as a function of the coupling laser Rabi frequency, at fixed Ω_p. (a) For NL product of 1.2×10^{14} cm^{-2}. (b) For NL product of 5.6×10^{14} cm^{-2}. The dashed vertical line in each figure is the value of Ω_c required for weak-probe EIT. The hyperbola is the $\alpha_T L \to \infty$ theoretical prediction of Eq. (2), taking Ω_p equal to (a) 0.25 cm^{-1} and (b) 0.24 cm^{-1}.

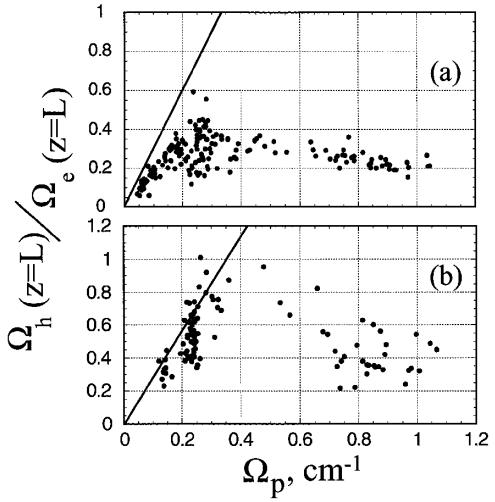

FIG. 3. Ratio of generated 186-nm and output 233-nm Rabi frequencies at the exit of the cell $\Omega_h(z = L)/\Omega_e(z = L)$, as a function of the probe laser Rabi frequency, at fixed Ω_c. (a) For NL product of 1.2×10^{14} cm^{-2}. (b) For NL product of 5.6×10^{14} cm^{-2}. The solid line is the $\alpha_T L \to \infty$ theoretical prediction, taking Ω_c equal to (a) 0.33 cm^{-1} and (b) 0.35 cm^{-1}.

are determined using the curve-of-growth method (to an accuracy of $\pm 10\%$). At 600 °C, the resonant absorption cross sections are $\sigma_e = 2.21 \times 10^{-13}$ cm^2 and $\sigma_h = 2.83 \times 10^{-13}$ cm^2. We investigate the behavior of the quadruply resonant, frequency converter at two density-length (NL) products: (a) 1.2×10^{14} cm^{-2} (588 °C) and (b) 5.6×10^{14} cm^{-2} (650 °C).

In Fig. 2, we study the dependence of the ratio of the Rabi frequencies of the generated VUV and output mixing fields at the exit of the sidearm cell, $\Omega_h(z = L)/\Omega_e(z = L)$, on the coupling laser Rabi frequency Ω_c. Here, the probe laser Rabi frequency is held at (a) 0.25 ± 0.01 cm^{-1} and (b) 0.24 ± 0.01 cm^{-1}, and $\Omega_e(0) < 0.025$ cm^{-1}. The curved, solid lines represent the theoretical prediction of Eqs. (2) at these values of Ω_p, assuming complete Rabi-frequency matching (i.e., taking $\alpha_T L \to \infty$). The dashed, vertical line indicates the coupling laser Rabi frequency at which, for each density, the step-up in EIT occurs (i.e., where, in the absence of the mixing laser, the transmission of a weak probe laser field through the cell exceeds 50%). Above this value, sufficient preparation energy has been applied to the system to ensure evolution of the ensemble into the population-trapped eigenstate [12]. In the following figures, only those points with $\Omega_c > 0.3$ cm^{-1} are shown.

In Fig. 3 we show $\Omega_h(z = L)/\Omega_e(z = L)$ as a function of the probe laser Rabi frequency Ω_p at fixed Ω_c and the $\alpha_T L \to \infty$ theoretical prediction. A striking feature of these data is the departure from theory when the Rabi frequency of the probe laser exceeds that of the coupling laser. This is most likely related to a failure of EIT; increasing the probe laser strength relative to the coupling laser in the presence of nonzero Raman-transition dephasing rates exacerbates two-photon absorption and causes non-negligible saturation and loss of coherence on time scales comparable to the pulse widths. (The dephasing time T_2 of the Raman transition coherence is $\approx$30 ns.) We expect that the use of shorter (but still adiabatic) pulses in such an experiment would limit this saturation and increase the strong-probe conversion efficiency. This strong-probe saturation behavior has been observed in other work in a continuous-wave regime [13]. We limit display of data in the remaining figures to those points where $\Omega_p < \Omega_c$.

In Fig. 4, we study the ratio of output and input mixing field Rabi frequencies $\Omega_e(z = L)/\Omega_e(0)$ as a function of

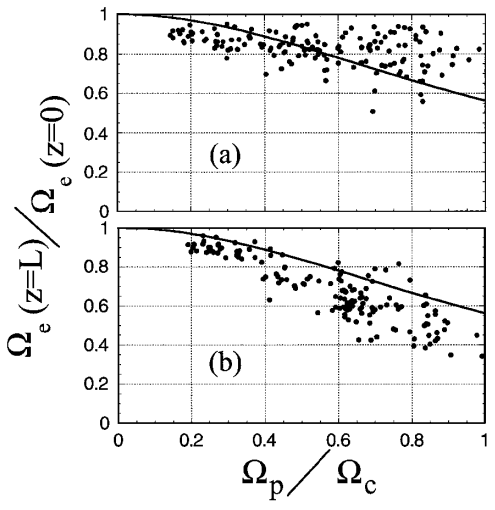

FIG. 4. Ratio of the output and input 233-nm Rabi frequencies $\Omega_e(z = L)/\Omega_e(z = 0)$ as a function of the ratio of probe and coupling laser Rabi frequencies Ω_p/Ω_c. (a) For NL product of 1.2×10^{14} cm^{-2}. (b) For NL product of 5.6×10^{14} cm^{-2}. The solid line is the $\alpha_T L \to \infty$ theoretical prediction.

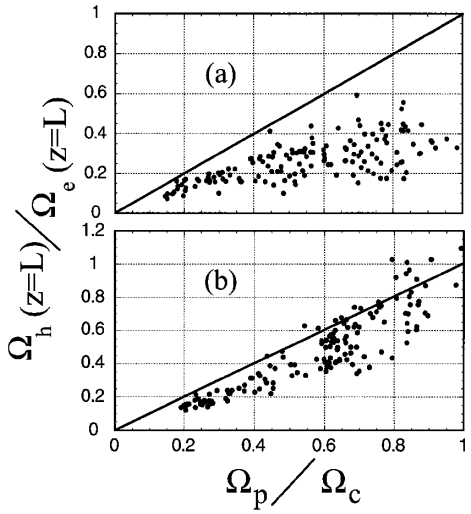

FIG. 5. Evolution to matched pulses. Ratio of generated 186-nm and output 233-nm Rabi frequencies at the exit of the cell $\Omega_h(z = L)/\Omega_e(z = L)$, as a function of the ratio of probe and coupling laser Rabi frequencies Ω_p/Ω_c. (a) For NL product of 1.2×10^{14} cm^{-2}. (b) For NL product of 5.6×10^{14} cm^{-2}. The solid line is the $\alpha_T L \to \infty$ theoretical prediction.

the ratio of the probe and coupling laser Rabi frequencies and compare with the predictions of Eq. (2b). Variation with the probe and coupling lasers is caused by the implicit dependence of the attenuation coefficients α_e and α_h on the population terms ρ_{22} and ρ_{11}. Note that, in the limit of weak probe (vanishing coherence), no population is transferred to state $|2\rangle$, and there is no appreciable absorption of the mixing field.

The data of the previous figures are combined in Fig. 5 to illustrate the evolution to a Rabi-frequency matching regime at the higher temperature. The opacity of the low density case ($\alpha_T L \approx 13$) should be more than sufficient to establish the Rabi-frequency matching condition, and no density dependence should remain. It is clear from the data, however, that matching is not attained until the higher density case ($\alpha_T L \approx 57$). The discrepancy arises from neglecting saturation and power broadening of the $|1\rangle \leftrightarrow |4\rangle$ and $|2\rangle \leftrightarrow |4\rangle$ transitions in the derivation of Eqs. (1). This assumption requires that the mixing and generated field Rabi frequencies Ω_e and Ω_h are both much less than the natural linewidth of the transitions. During the experiment, the intensities of these fields are usually an order of magnitude larger than the saturation intensities. We identify power broadening by the 233-nm field and the resulting decrease in the number of absorption depths at both ω_e and ω_h as the primary saturation mechanism in this experiment. Close agreement between numerical simulation and experimental results is obtained if the small-signal absorption coefficients α_e and α_h are replaced by their power-broadened values. Saturation is most evident in the behavior of the conversion efficiency from $\omega_e \rightarrow \omega_h$; small-signal efficiencies [$\Omega_e(0) < 0.005$ cm^{-1}] exceed 30% but drop sharply to between 5% and 10% when $\Omega_e(0)$ is raised to 0.02 cm^{-1} because the effective opacity is progressively reduced to the point where the matching condition is no longer attained.

At the higher NL condition, we achieved approximately 1% overall energy conversion efficiency. A VUV pulse energy of 1 μJ was generated using 10 μJ of 233 nm and 50 μJ each of 283 and 406 nm.

In summary, we have demonstrated efficient nonlinear frequency conversion in a quadruply resonant double-Λ atomic system, using collimated laser fields with modest power densities. This work provides the first experimental realization of nonlinear optics in a density-invariant, Rabi-frequency matching regime. Three resonant, arbitrarily phased fields are applied at $z = 0$, and after a characteristic distance, the atom renders itself transparent to all fields through generation of a properly phased, fourth resonant field. Transparency is achieved once the complex ratio of Rabi frequencies in each Λ-channel is equal, and once transparent, no further changes to relative phase or amplitude occur. The overall conversion efficiencies of these all-resonant frequency converters are limited by the preparation energy requirement necessary to establish EIT in the first Λ-channel and by power broadening of the second Λ-channel. We note that the use of a single-isotope atomic medium minimizes the required values of Ω_c [14] but is otherwise unnecessary.

The authors thank H. Xia for experimental assistance and J. Reader and R. Englemann at Opthos Instruments for construction and filling of the custom sidearm cells. This work was supported by the U.S. Air Force Office of Scientific Research, the U.S. Army Research Office, and the U.S. Office of Naval Research.

Note added in proof.—A comprehensive theoretical study of nonlinear optics in double-Λ atomic systems, with emphasis on pulse-matching properties, has recently been published by Korsunsky *et al.* [15].

[1] M. Jain, H. Xia, G. Y. Yin, A. J. Merriam, and S. E. Harris, Phys. Rev. Lett. **77**, 4326 (1996); M. Jain, J. E. Field, and G. Y. Yin, Opt. Lett. **18**, 998 (1993).

[2] A. J. Merriam, S. J. Sharpe, H. Xia, D. Manuszak, G. Y. Yin, and S. E. Harris, Opt. Lett. **24**, 625 (1999); A. J. Merriam, S. J. Sharpe, H. Xia, D. Manuszak, G. Y. Yin, and S. E. Harris, IEEE J. Sel. Top. Quantum Electron. **5**, 1502 (1999).

[3] K. Hakuta, M. Suzuki, M. Katsuragawa, and J. Z. Li, Phys. Rev. Lett. **79**, 209 (1997).

[4] See, e.g., E. Arimondo, in *Progress in Optics*, edited by E. Wolf (North-Holland, Amsterdam, 1996), Vol. XXXV, and references therein.

[5] S. Y. Zhu, M. O. Scully, H. Fearn, and L. M. Narducci, Z. Phys. D **22**, 483 (1992); M. Fleischhauer and M. O. Scully, Opt. Commun. **105**, 79 (1994); O. Kocharovskara and P. Mandel, Phys. Rev. A **42**, 523 (1990).

[6] Experimental work is described by B. Lu, W. H. Burkett, and M. Xiao, Opt. Lett. **23**, 804 (1998); S. Babin, U. Hinze, E. Tinemann, and B. Wellehehausen, Opt. Lett. **21**, 1186 (1996); P. R. Hemmer *et al.*, Opt. Lett. **20**, 982 (1995); A. S. Zibrov, M. D. Lukin, and M. O. Scully, Phys. Rev. Lett. **83**, 4049 (1999). A theoretical study was undertaken by M. D. Lukin, P. R. Hemmer, M. Loeffler, and M. O. Scully, Phys. Rev. Lett. **81**, 2675 (1998).

[7] S. E. Harris, Phys. Rev. Lett. **70**, 552 (1993).

[8] See, e.g., A. V. Smith, W. J. Alford, and G. R. Hadley, J. Opt. Soc. Am. B **5**, 1503 (1988), and references therein.

[9] A. Kasapi, M. Jain, and G. Y. Yin, Appl. Phys. Lett. **35**, 1999 (1996); A. J. Merriam and G. Y. Yin, Opt. Lett. **23**, 1034 (1998).

[10] The fluorescence quantum efficiency is the same at 233 and 186 nm; see, e.g., J. A. R. Samson, *Techniques of Vacuum Ultraviolet Spectroscopy* (Pied Publications, Lincoln, Nebraska, 1967).

[11] A. Kasapi, M. Jain, G. Y. Yin, and S. E. Harris, Phys. Rev. Lett. **74**, 2447 (1995); M. Jain, A. J. Merriam, A. Kasapi, G. Y. Yin, and S. E. Harris, Phys. Rev. Lett. **75**, 4385 (1995).

[12] S. E. Harris and Z. F. Luo, Phys. Rev. A **52**, R928 (1995).

[13] S. Wielandy and A. L. Gaeta, Phys. Rev. A **58**, 2500 (1998).

[14] H. Xia, A. J. Merriam, S. J. Sharpe, G. Y. Yin, and S. E. Harris, Phys. Rev. A **59**, R3190 (1999).

[15] E. A. Korsunsky and D. V. Kosachiov, Phys. Rev. A **60**, 4996 (1999).